Sodium-Ion Batteries | Hot Paper

DOI: 10.1002/anie.201407898

MoS_2 Nanoflowers with Expanded Interlayers as High-Performance Anodes for Sodium-Ion Batteries**

*Zhe Hu, Lixiu Wang, Kai Zhang, Jianbin Wang, Fangyi Cheng, Zhanliang Tao, and Jun Chen**

Abstract: *MoS_2 nanoflowers with expanded interlayer spacing of the (002) plane were synthesized and used as high-performance anode in Na-ion batteries. By controlling the cut-off voltage to the range of 0.4–3 V, an intercalation mechanism rather than a conversion reaction is taking place. The MoS_2 nanoflower electrode shows high discharge capacities of 350 mAh g^{-1} at 0.05 A g^{-1}, 300 mAh g^{-1} at 1 A g^{-1}, and 195 mAh g^{-1} at 10 A g^{-1}. An initial capacity increase with cycling is caused by peeling off MoS_2 layers, which produces more active sites for Na^+ storage. The stripping of MoS_2 layers occurring in charge/discharge cycling contributes to the enhanced kinetics and low energy barrier for the intercalation of Na^+ ions. The electrochemical reaction is mainly controlled by the capacitive process, which facilitates the high-rate capability. Therefore, MoS_2 nanoflowers with expanded interlayers hold promise for rechargeable Na-ion batteries.*

Na-ion batteries (NIBs) have recently attracted great interest due to the cheap raw material.[1] However, compared to Li-ion batteries (LIBs), the larger diameter of the sodium ion hampers electrochemical reaction kinetics, which makes it difficult to find suitable host materials for reversible and rapid Na^+ insertion and extraction.[2] Particularly for the anode materials of NIBs, the main problems include large voltage polarization and bad cycling performance.[3] Recent studies have shown that in NIBs, the anode materials following the alloy-type (Sn and SnO_2)[4] and conversion-type mechanism (CuO and FeS_2)[5] exhibited high initial capacity but suffered from poor cycling performance owing to the large volume change or the sluggish kinetics.[6] For materials dominated by the intercalation mechanism, such as $Na_3V_2(PO_4)_3$ and P2-type $Na_{0.66}[Li_{0.22}Ti_{0.78}]O_2$,[7] the cyclability has been improved, however, their specific capacity is still limited. Therefore, it is desirable to find appropriate anode materials with both high capacity and long cycling life.

MoS_2, which has a well-defined layered structure,[8] has been intensively investigated as anode material for rechargeable batteries.[9] According to the terminal discharge voltage, the reactions in a Na-MoS_2 battery proceed in two steps, that is, intercalation and conversion as shown in Equation (1) and (2), respectively.[10]

$$MoS_2 + xNa = Na_xMoS_2 \text{ (above 0.4 V, } x < 2) \quad (1)$$

$$Na_xMoS_2 + (4-x)Na = Mo + 2Na_2S \text{ (below 0.4 V)} \quad (2)$$

In the conversion-type reaction [Eq. (2)] bare MoS_2 will be fully converted to Mo metal and sodium sulfide, resulting in bad electrochemical performance.[11] Maier's group has improved the conversion-type reaction by employing ultrasmall MoS_2 nanoplates in carbon nanofibers.[12] The as-prepared sample displayed a remarkable discharge capacity of 436 mAh g^{-1} at 1 A g^{-1}. However, the capacity dropped to 57% after 100 cycles. Bang et al. optimized the cycling performance with nearly no capacity loss for 100 cycles by using layered MoS_2 nanosheets and controlling the terminal voltage to 0.4 V.[13] The discharge capacity of their device was only 165 mAh g^{-1}, thus improving the discharge capacity is still an urgent task.

MoS_2 with expanded interlayers have often been used for enhancing the discharge capacity and reaction kinetics in LIBs,[14] and graphite with expanded interlayers also contributes to the enhancement of anode performance in NIBs.[15] Here, we report the synthesis of graphene-like MoS_2 nanoflowers with expanded interlayers and their application as high-performance anode in rechargeable Na-ion batteries. In particular, controlling the voltage range of 0.4–3 V preserves the layer structure between MoS_2 and Na_xMoS_2 through the intercalation reaction shown in Equation (1). This delivers an initial capacity increase with cycling due to the exfoliation of MoS_2 layers to produce more active reaction sites for Na^+ storage.

Graphene-like MoS_2 nanoflowers (FG-MoS_2) were synthesized by a hydrothermal method and treated by freeze-drying. After annealing at 700 °C for 3 h, FG-MoS_2 turned into well-crystallized MoS_2 (labeled as CG-MoS_2). Bulk MoS_2 (Alfa Aesar, B-MoS_2) was purchased for comparison. Figure 1a shows the X-ray diffraction (XRD) patterns of as-prepared samples. All the characteristic peaks match with JCPDS No. 37-1492, however, for FG-MoS_2 the peak of the (002) plane shows a small shift to low scattering angle, which is ascribed to the intercalation of Na^+ and NH_4^+ in the MoS_2 (002) layers during the hydrothermal process.[16] Compared with the broadened peaks of FG-MoS_2, CG-MoS_2 shows sharper peaks, indicating a closer arrangement of the crystal structure in CG-MoS_2, leading to a slight decrease of the interplanar spacing in CG-MoS_2.[17] Figure 1b–d show the high resolution transmission electron microscope (HRTEM) images of FG-MoS_2, CG-MoS_2, and B-MoS_2. FG-MoS_2 and

[*] Z. Hu, L. Wang, Dr. K. Zhang, Dr. J. Wang, Prof. F. Cheng, Prof. Z. Tao, Prof. J. Chen
Key Laboratory of Advanced Energy Materials Chemistry (Ministry of Education), Collaborative Innovation Center of Chemical Science and Engineering, College of Chemistry, Nankai University
Tianjin 300071 (China)
E-mail: chenabc@nankai.edu.cn

[**] This work was supported by the 973 Program (2011CB935900), the NSFC (21231005 and 51231003), and the MOE Project (B12015 and IRT13R30).

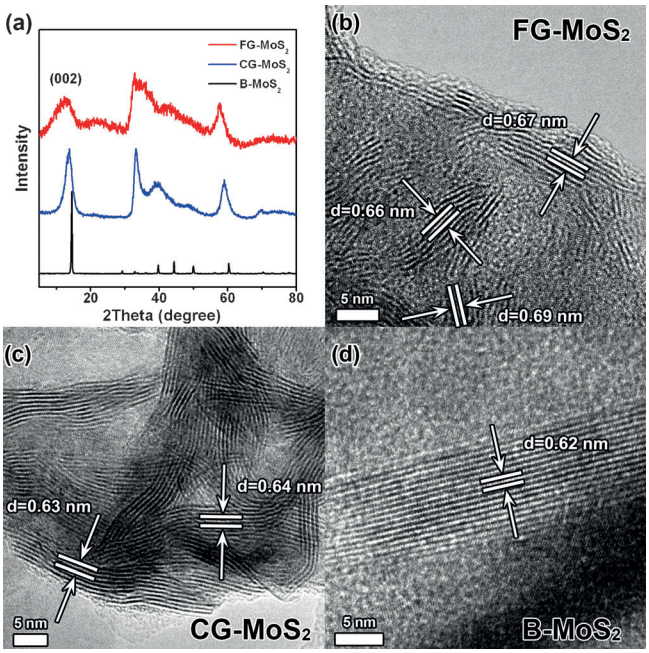

Figure 1. a) XRD patterns of the MoS_2 samples and HRTEM images of b) FG-MoS_2, c) CG-MoS_2, and d) B-MoS_2.

CG-MoS_2 have expanded interlayers (0.67 nm and 0.64 nm, respectively) in comparison to B-MoS_2 (0.62 nm). The layers of FG-MoS_2 and CG-MoS_2 are distorted, while the layers of B-MoS_2 exhibit a well-crystallized structure. FG-MoS_2 and CG-MoS_2 are nanoflowers that are wrinkled and thin as graphene (Figures S1 and S2a,b). In contrast, B-MoS_2 has large particle size of 10–20 μm (Figure S2c). Raman spectra of FG-MoS_2, CG-MoS_2, and B-MoS_2 were recorded (Figure S2d). Raman peaks around 404 cm^{-1} and 379 cm^{-1} correspond to the A_{1g} and E^1_{2g} vibration modes, respectively. Compared to B-MoS_2, the synthesized FG-MoS_2 and CG-MoS_2 show broadened peaks and short peak distances, indicating that the as-prepared samples have smaller particle size and fewer layer number.[18]

Figure 2a shows the initial discharge/charge curves of FG-MoS_2, CG-MoS_2, and B-MoS_2 in the voltage range of 0.4–3.0 V at 0.2 A g^{-1}. The discharge capacities of FG-MoS_2, CG-MoS_2, and B-MoS_2 are 243, 218, and 160 mAh g^{-1}, respectively. As can be seen from the cyclic voltammetry curves in the 1st cycle (Figure S3), FG-MoS_2 shows the lowest voltage polarization, the highest Na^+ insertion platform, and the highest coulombic efficiency (Table S1). Such phenomenon has already been observed in Li-MoS_2 batteries.[17] As the lattice distance of the (002) plane gets larger, the discharge platform turns higher, which can be attributed to the low energy barrier of Na^+ intercalation into the MoS_2 layers.[9d,14b] The remarkable rate performance of FG-MoS_2 is shown in Figure 2b. The reversible discharge capacities of FG-MoS_2 are 200 mAh g^{-1} at 1 A g^{-1} and 175 mAh g^{-1} at a relatively

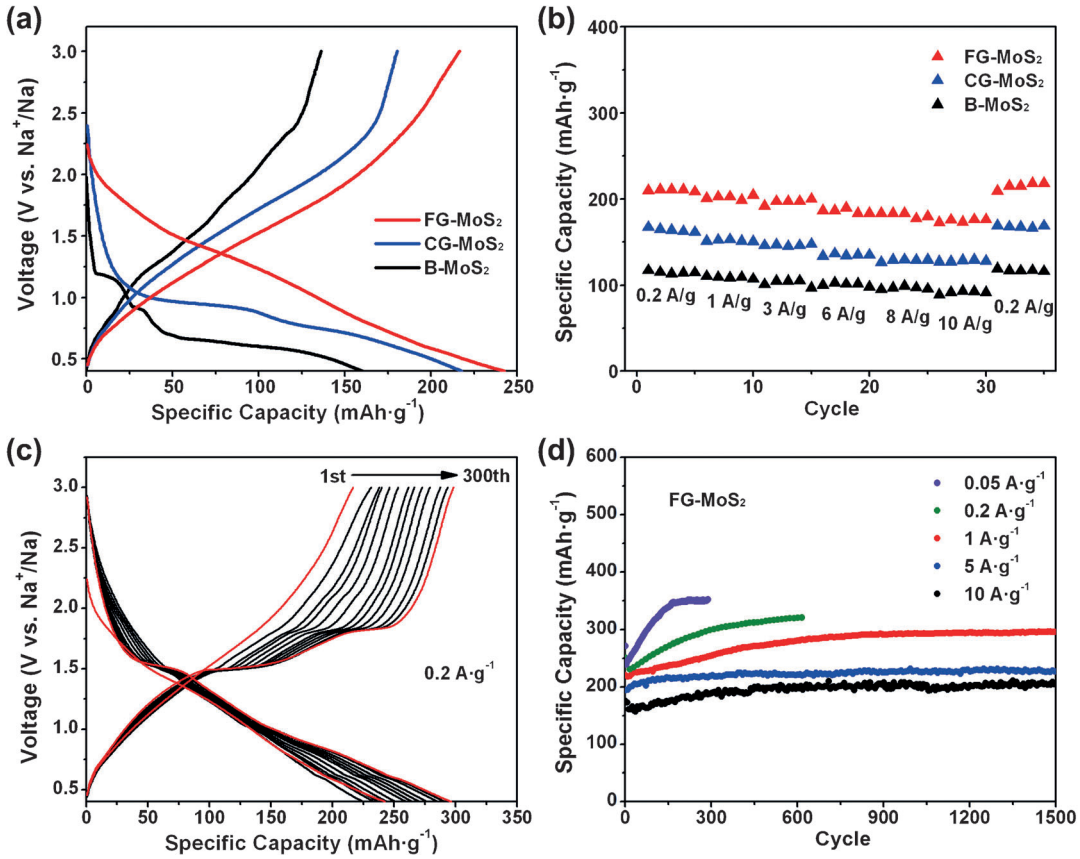

Figure 2. Electrochemical tests: a) Charge and discharge curves of the as-prepared FG-MoS_2, CG-MoS_2, and B-MoS_2 at the first cycle. b) The rate performance. c) The charge and discharge curves from 1st to 300th cycle and d) the cyclic properties at different rates of FG-MoS_2.

high rate of 10 $A g^{-1}$, which is much better than that of the other two samples (CG-MoS_2 and B-MoS_2). The rate performance of FG-MoS_2, CG-MoS_2, and B-MoS_2 is coincident with the interlayer distance from large to small, indicating that a larger interlayer distance leads to faster reaction kinetics.

Further cycling tests were carried out to investigate the cyclability of FG-MoS_2. Figure 2c shows the cell cycling at 0.2 $A g^{-1}$ for 300 cycles. Interestingly, the discharge capacity increases slowly from 220 to 295 $mAh g^{-1}$, and the curves at the 300th cycle display much smaller polarization than the original curves. (Figure S4). This kind of capacity increasing disappears at ca. 200 cycles for low current densities of 0.05–0.2 $A g^{-1}$ and at ca. 500 cycles for high current densities of 1–10 $A g^{-1}$. Finally, the reversible discharge capacities maintain 350 $mAh g^{-1}$ at 0.05 $A g^{-1}$, 300 $mAh g^{-1}$ at 1 $A g^{-1}$, and 195 $mAh g^{-1}$ at 10 $A g^{-1}$ (Figure 2d). The increased capacity should be derived from the gradually expanded and exfoliated interlayers, which actually provide more active Na^+ storage sites and low energy barrier for Na^+ to intercalation or deintercalation. For comparison, a stability test of FG-MoS_2 at 0.1–3 V is shown in Figure S5. The initial discharge capacity was 481 $mAh g^{-1}$ (i.e., 2.9 e^-). However, the cell suffered from a bad cycling performance (Figure S5b). Therefore, controlling the terminal voltage to 0.4 V is important for Na-MoS_2 batteries, particularly for bare MoS_2 that is not composited with carbon.

We used electrochemical impedance spectroscopy (EIS), cyclic voltammetry (CV), and HRTEM to explain the electrochemical features of FG-MoS_2 such as the high-rate ability, high discharge capacity, and stable cyclability. EIS measurements were performed during the first cycling of the FG-MoS_2-Na cell (Figure S6). The charge transfer resistance (R_{ct}, which value depends on the diameter of the semicircle)[19] becomes smaller when Na^+ ions insert into the MoS_2 layers and gets larger when Na^+ ions extract out (for details see Table S2). For layered materials, R_{ct} correlates with the Fermi level and free-electron concentration.[16,20] Thus, preservation of the layered structure should enhance the rate properties of MoS_2-Na cells.

Figure 3a displays the cyclic voltammograms of an FG-MoS_2 battery that cycles 1000 times at different sweep rates from 0.1 to 1.0 $mV s^{-1}$. Peaks in the CV curves are consistent with the stable discharge–charge curves at the 300th cycle in Figure 2c. The results show that the peak current density is not proportional to the square root of the sweep rate. A similar observation was made in previous studies on LIBs.[21] The charge storage mechanism of nanosized particles always contains non-faradaic and faradaic processes. The former mainly exists in the double layer capacitors. The latter is found both in the bulk as a battery process and on the surface as Pseudocapacitance. The capacitive effect of the battery system is calculated according to Equations (3) and (4):

$$i = a v^b \quad (3)$$

$$\log i = b \times \log v + \log a \quad (4)$$

where i is the current density, v is the scan rate, and a and b are adjustable parameters. When the b-value approaches 1, the system is mainly controlled by capacitance, and when the b-value is close to 0.5, the Na^+ insertion process dominates. Figure 3b shows the $\log i$ vs. $\log v$ plots at different oxidation or reduction state. As the b-value approaches 1, the Na-MoS_2 battery is mainly controlled by the capacitive process. This leads to a fast Na^+ insertion/extraction (high rate property) and extended cycling life.

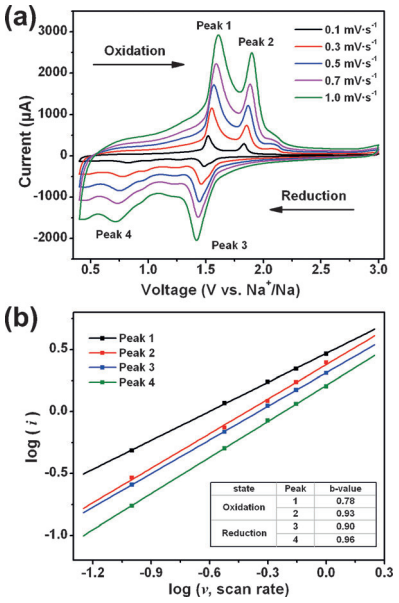

Figure 3. a) CV curves at different scan rate of FG-MoS_2 after 1000 cycles and b) $\log i$ vs. $\log v$ plots at different oxidation and reduction states.

Further, we recorded HRTEM images of the discharged MoS_2 electrode after the 10th, 500th, and 1000th cycle. The HRTEM image after the 10th cycle (Figure 4a) shows that the MoS_2 layers were more expanded and flexible than the original MoS_2. After 500 cycles (Figure 4b), the MoS_2 layers were even more expanded. After 1000 cycles (Figure 4c), many of the MoS_2 layers are separated into single layers or bilayers, leading to a large specific surface area. This phenomenon is uncommon for Li-MoS_2 or Na-MoS_2 batteries with cut-off voltages up to 0.1 V, where the conversion mechanism completely destroys the layer structure and generates Mo metal embedded in a Na_2S matrix (Figure S7). Mo metal is also detected in the charged state, which means that the separation of the metal and sulfide phases is hardly reversible, which leads to a severe capacity decay.[12] However, in a Na-MoS_2 battery with cut-off voltage up to 0.4 V, an intercalation mechanism is getting dominant. The schematic illustration shown in Figure S8 is simulating the Na^+ storage situation and the change of MoS_2 layers during cycling. The repetition of Na^+ insertion and extraction results in both the increase of the interlayer spacing and the decrease of the layer numbers in MoS_2. This provides a lower energy barrier for Na^+ insertion, more active reaction sites for Na^+ storage,[9d,22] and thus the capacity increase with cycling.

In conclusion, MoS_2 nanoflowers with expanded layers show high-performance as the anode material for Na-ion

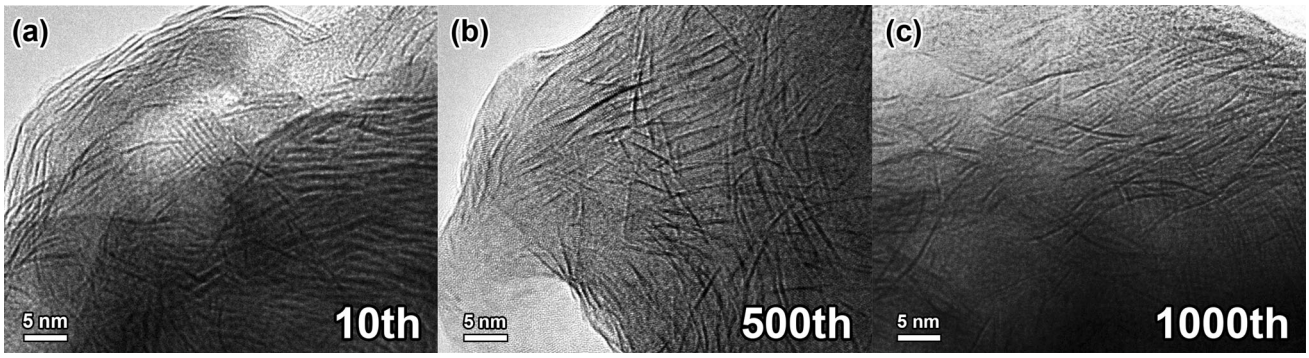

Figure 4. HRTEM images of the electrode material after discharging to 0.4 V in MoS_2-Na battery after a) 10, b) 500, and c) 1000 cycles.

batteries. By controlling the cut-off voltage to 0.4 V, the Na-MoS_2 battery follows an intercalation-type reaction with improved cyclic performance. The expanded and gradually exfoliated interlayers contribute to a lowering of the Na^+ insertion and extraction barrier, thus reducing the charge transfer resistance and providing more active sites for Na^+ storage. Moreover, the capacitive controlled reaction accelerates the diffusion of Na^+ and e^-, fundamentally improving the rate property. Such long-life anode material with high rate property and stable cyclability is promising for rechargeable Na-ion batteries.

Received: August 3, 2014
Published online: September 22, 2014

Keywords: electrochemical exfoliation · expanded layers · MoS_2 · pseudocapacitance · sodium-ion batteries

[1] a) J. M. Tarascon, *Nat. Chem.* **2010**, *2*, 510 – 510; b) S.-W. Kim, D.-H. Seo, X. H. Ma, G. Ceder, K. Kang, *Adv. Energy Mater.* **2012**, *2*, 710 – 721; c) M. D. Slater, D. Kim, E. Lee, C. S. Johnson, *Adv. Funct. Mater.* **2013**, *23*, 947 – 958.

[2] V. Palomares, M. Casas Cabanas, E. Castillo Martinez, M. H. Han, T. Rojo, *Energy Environ. Sci.* **2013**, *6*, 2312 – 2337.

[3] J. F. Qian, X. Y. Wu, Y. L. Cao, X. P. Ai, H. X. Yang, *Angew. Chem. Int. Ed.* **2013**, *52*, 4633 – 4636; *Angew. Chem.* **2013**, *125*, 4731 – 4734.

[4] a) Y. H. Liu, Y. H. Xu, Y. J. Zhu, J. N. Culver, C. A. Lundgren, K. Xu, C. S. Wang, *ACS Nano* **2013**, *7*, 3627 – 3634; b) Y. H. Xu, Y. J. Zhu, Y. H. Liu, C. Wang, *Adv. Energy Mater.* **2013**, *3*, 128 – 133; c) Y. Wang, D. W. Su, C. Y. Wang, G. X. Wang, *Electrochem. Commun.* **2013**, *29*, 8 – 11.

[5] a) L. J. Wang, K. Zhang, Z. Hu, W. C. Duan, F. Y. Cheng, J. Chen, *Nano Res.* **2014**, *7*, 199 – 208; b) A. Kitajou, J. Yamaguchi, S. Hara, S. Okada, *J. Power Sources* **2014**, *247*, 391 – 395; c) Z. L. Jian, P. Liu, F. J. Li, M. W. Chen, H. S. Zhou, *J. Mater. Chem. A* **2014**, *2*, 13805 – 13809.

[6] a) M. T. McDowell, S. W. Lee, J. T. Harris, B. A. Korgel, C. M. Wang, W. D. Nix, Y. Cui, *Nano Lett.* **2013**, *13*, 758 – 764; b) K. Zhang, X. P. Han, Z. Hu, X. L. Zhang, Z. L. Tao, J. Chen, *Chem. Soc. Rev.* **2014**, DOI: 10.1039/c4cs00218k.

[7] a) Y. Sun, L. Zhao, H. L. Pan, X. Lu, L. Gu, Y. S. Hu, H. Li, M. Armand, Y. Ikuhara, L. Q. Chen, X. J. Huang, *Nat. Commun.* **2013**, *4*, 1870; b) W. C. Duan, Z. Q. Zhu, H. Li, Z. Hu, K. Zhang, F. Y. Cheng, J. Chen, *J. Mater. Chem. A* **2014**, *2*, 8668 – 8675; c) Y. S. Wang, X. Q. Yu, S. Y. Xu, J. M. Bai, R. J. Xiao, Y. S. Hu, H. Li, X. Q. Yang, L. Q. Chen, X. J. Huang, *Nat. Commun.* **2013**, *4*, 2365; d) H. J. Yu, Y. Ren, D. D. Xiao, S. H. Guo, Y. B. Zhu, Y. M. Qian, L. Gu, H. S. Zhou, *Angew. Chem. Int. Ed.* **2014**, *53*, 8963 – 8969; *Angew. Chem.* **2014**, *126*, 9109 – 9115.

[8] a) R. Tenne, *Nat. Nanotechnol.* **2006**, *1*, 103 – 111; b) F. Y. Cheng, J. Chen, X. L. Gou, *Adv. Mater.* **2006**, *18*, 2561 – 2564; c) H. Li, J. Wu, Z. Y. Yin, H. Zhang, *Acc. Chem. Res.* **2014**, *47*, 1067 – 1075; d) Z. Y. Zeng, Z. Y. Yin, X. Huang, H. Li, Q. Y. He, G. Lu, F. Boey, H. Zhang, *Angew. Chem. Int. Ed.* **2011**, *50*, 11093 – 11097; *Angew. Chem.* **2011**, *123*, 11289 – 11293; e) M. Chhowalla, H. S. Shin, G. Eda, L. J. Li, K. P. Loh, H. Zhang, *Nat. Chem.* **2013**, *5*, 263 – 275.

[9] a) J. Chen, N. Kuriyama, H. T. Yuan, H. T. Takeshita, T. Sakai, *J. Am. Chem. Soc.* **2001**, *123*, 11813 – 11814; b) Y. L. Liang, R. J. Feng, S. Q. Yang, H. Ma, J. Liang, J. Chen, *Adv. Mater.* **2011**, *23*, 640 – 643; c) L. C. Yang, S. N. Wang, J. J. Mao, J. W. Deng, Q. S. Gao, Y. Tang, O. G. Schmidt, *Adv. Mater.* **2013**, *25*, 1180 – 1184; d) J. Xiao, X. J. Wang, X. Q. Yang, S. D. Xun, G. Liu, P. K. Koech, J. Liu, J. P. Lemmon, *Adv. Funct. Mater.* **2011**, *21*, 2840 – 2846; e) X. H. Cao, Y. M. Shi, W. H. Shi, X. H. Rui, Q. Y. Yan, J. Kong, H. Zhang, *Small* **2013**, *9*, 3433 – 3438; f) X. Huang, Z. Y. Zeng, H. Zhang, *Chem. Soc. Rev.* **2013**, *42*, 1934 – 1946; g) X. Huang, C. L. Tan, Z. Y. Yin, H. Zhang, *Adv. Mater.* **2014**, *26*, 2185 – 2204.

[10] a) L. David, R. Bhandavat, G. Singh, *ACS Nano* **2014**, *8*, 1759 – 1770; b) J. S. Park, J. S. Kim, J. W. Park, T. H. Nam, K. W. Kim, J. H. Ahn, G. X. Wang, H. J. Ahn, *Electrochim. Acta* **2013**, *92*, 427 – 432.

[11] Y. X. Wang, S. L. Chou, D. Wexler, H. K. Liu, S. X. Dou, *Chem. Eur. J.* **2014**, *20*, 9607 – 9612.

[12] C. B. Zhu, X. K. Mu, P. A. van Aken, Y. Yu, J. Maier, *Angew. Chem. Int. Ed.* **2014**, *53*, 2152 – 2156; *Angew. Chem.* **2014**, *126*, 2184 – 2188.

[13] G. S. Bang, K. W. Nam, J. Y. Kim, J. Shin, J. W. Choi, S. Y. Choi, *ACS Appl. Mater. Interfaces* **2014**, *6*, 7084 – 7089.

[14] a) H. Liu, D. W. Su, R. F. Zhou, B. Sun, G. X. Wang, S. Z. Qiao, *Adv. Energy Mater.* **2012**, *2*, 970 – 975; b) G. D. Du, Z. P. Guo, S. Q. Wang, R. Zeng, Z. X. Chen, H. K. Liu, *Chem. Commun.* **2010**, *46*, 1106 – 1108; c) H. Hwang, H. Kim, J. Cho, *Nano Lett.* **2011**, *11*, 4826 – 4830.

[15] Y. Wen, K. He, Y. J. Zhu, F. D. Han, Y. H. Xu, I. Matsuda, Y. Ishii, J. Cumings, C. S. Wang, *Nat. Commun.* **2014**, *5*, 4033.

[16] A. Zak, Y. Feldman, V. Lyakhovitskaya, G. Leitus, R. Popovitz Biro, E. Wachtel, H. Cohen, S. Reich, R. Tenne, *J. Am. Chem. Soc.* **2002**, *124*, 4747 – 4758.

[17] K. Chang, W. X. Chen, L. Ma, H. Li, H. Li, F. H. Huang, Z. D. Xu, Q. B. Zhang, J. Y. Lee, *J. Mater. Chem.* **2011**, *21*, 6251 – 6257.

[18] H. S. S. Ramakrishna Matte, A. Gomathi, A. K. Manna, D. J. Late, R. Datta, S. K. Pati, C. N. R. Rao, *Angew. Chem. Int. Ed.* **2010**, *49*, 4059 – 4062; *Angew. Chem.* **2010**, *122*, 4153 – 4156.
[19] Z. Hu, K. Zhang, H. Y. Gao, W. C. Duan, F. Y. Cheng, J. Liang, J. Chen, *J. Mater. Chem. A* **2013**, *1*, 12650 – 12656.
[20] S. Q. Yang, D. X. Li, T. R. Zhang, Z. L. Tao, J. Chen, *J. Phys. Chem. C* **2012**, *116*, 1307 – 1312.
[21] a) T. Brezesinski, J. Wang, S. H. Tolbert, B. Dunn, *Nat. Mater.* **2010**, *9*, 146 – 151; b) J. Wang, J. Polleux, J. Lim, B. Dunn, *J. Phys. Chem. C* **2007**, *111*, 14925 – 14931.
[22] K. Chang, W. X. Chen, *J. Mater. Chem.* **2011**, *21*, 17175 – 17184.

